Environmental Protection Research
http://ojs.wiserpub.com/index.php/EPR/

UNIVERSAL WISER PUBLISHER

Research Article

Locally Sourced Charcoal Removes Excess Fe from Seawater - Effect of Sorbent Size on the Adsorption Properties

Adedeji A. Adelodun*, Ebenezer Akinbobola, Nasifudeen O. Afolabi

Department of Marine Science & Technology, School of Earth & Mineral Sciences, The Federal University of Technology, Akure, Nigeria
E-mail: aaadelodun@futa.edu.ng

Received: 19 December 2021; **Revised:** 20 January 2022; **Accepted:** 24 March 2022

Abstract: The status quo of the iron (Fe) concentration in the seawater (0.55 mg/L) of the Araromi coastal area in Nigeria exceeds the permissible limit set by the World Health Organization (WHO; 0.3 mg/L) for drinking water. To lower the Fe content, the adsorption potential of locally sourced mangrove wood-based charcoal (WC) with three particle sizes (0.38dp, 1.18dp, and 2.00dp) was investigated, where dp means particle diameter in mm, under varied parameters (dosages, contact time, and temperature). The adsorption efficiency (ζ) improved with an increase in each parameter. The WC with a particle size of 0.38dp evinced the highest ζ (91.0%, 88.8%, and 81.1%) under the parameters of 60 g/L dosage, 50 min of contact time, and 60 °C of temperature, respectively. Generally, the ζ followed the order of 0.38dp > 1.18dp > 2.00dp. Through modeling, 0.38dp WC would achieve an ζ of 100% if the dosage, contact time, and temperature were 4.04 g/L, 56 min, and 81.2 °C, respectively. Furthermore, the adsorption favored the Freundlich model (R^2 = 0.893 – 0.999) over the Langmuir model (R^2 = 0.558 – 0.994), fitting pseudo-second-order (R^2 = 0.974 – 0.992) rather than pseudo-first-order (R^2 = 0.804 – 0.989) kinetics. Also, the predominance of chemisorption over physisorption was established by the enthalpy change value (ΔH = 19.05 – 40.47 kJ/mol). The Fe adsorption was thermodynamically feasible (ΔG = -10.3 – -7.3 kJ/mol) and endothermic, confirming the positive linearity between ζ and temperature. Consequently, low-cost, readily available WC was effective in lowering the Fe levels in seawater to a potable level.

***Keywords*:** removal efficiency, isotherm, kinetics, thermodynamics, water quality

1. Introduction

Trace (toxic) metals (such as copper, zinc, lead, mercury, cadmium, arsenic, carbon monoxide, iron, etc.) are non-biodegradable inorganic pollutants, usually produced from various anthropogenic activities [1,2]. When present in the environment above absorbable and adaptable levels, they could harm the ecosystem, including humans. In the human system, toxic metals may cause several illnesses, such as dehydration, abdominal pain, diarrhea, numbness, cardiac failure, confusion, brain damage, itai-itai, psychosis, etc. [3,4]. Although iron (Fe) deficiency in humans may hinder blood clotting, its ingestion at elevated levels causes gastrointestinal and cardiovascular collapse [5].

The corrosion of abandoned ship wreckages, oil pipes, dumped industrial metal scraps, and underwater cables could increase Fe levels in seawater and coastal water bodies beyond permissible environmental limits [6]. Therefore, there is a need to control Fe levels in such estuaries and seawater where the Fe levels usually exceed potable water

DOI: https://doi.org/10.37256/epr.2120221284

standards (< 0.3 mg/L).

The conventional chemical techniques for trace metal control include precipitation, ion exchange [7], electro-coagulation [8], membrane separation [9], reverse osmosis [10], electrodialysis [11], solvent extraction [12], phytoextraction [13], ultrafiltration [14], adsorption, etc. [15-17]. Adsorption has numerous merits compared to these options, such as high cost effectiveness, high reusability of sorbents, easy application, excellent efficiency, etc. However, some rural areas in underdeveloped and developing countries (such as seaside settlements in the oil-rich Niger-Delta regions of Nigeria) lack access to factory-made adsorbents (such as activated carbon, activated carbon fibers, molecular sieves, metal-organic frameworks, etc.) to purify their polluted waters before consumption.

Baruah et al. [18] carried out Fe removal in an indigenous water filtration system in Assam, Northeastern India. The various Bambusa charcoals reduced Fe concentration (0.3 to 4 mg/L) by 56.3% to 74.24% at pH 7.5. Elsewhere, Aji and co-researchers [19] applied activated carbon to remove Fe from Alau Dam in Maiduguri, Nigeria. The sorbent reduced the initial Fe concentration (3.11 mg/L) by 90% after 50 min. In the same year, Fe (along with aluminium and manganese) was removed from industrial waste using activated carbon and an ion-exchanger (Amberlite IR-120H) [20]. With 2 g/L dosage, pH of 7, and 30 min contact time, 99.02% Fe removal efficiency was achieved. The removal mechanism also favored the Langmuir model over Freundlich. Recently, Fe was adsorbed from groundwater using ash from five different sources, i.e., banana rind, banana leaf, banana pseudostem, rice husk, and bamboo [21]. The researchers found banana pseudostem-derived ash to be the most efficient option, lowering the original Fe level from 2.2 to 0.3 ppm.

Because of the high poverty level and the huge amount of adsorbents incessantly needed by the coastal settlers to purify their waters, research attention has shifted toward using low-cost and readily available adsorbents such as orange peel, sawdust, coconut waste, sugarcane bagasse, rice husk, amongst others [22]. However, considering that fish smoking is the primary occupation of the coastal residents, no research has delved into the use of unmodified charcoal (constantly obtained from fish smoking) to remove Fe (being the most abundant trace metal in the wastewater and seawater). Therefore, in this study, the potential of readily available mangrove wood-based charcoal (WC) to remove excess Fe from polluted waters was evaluated, especially for the residents of the region who don't have enough water for municipal and nutritional needs.

2. Materials and methods

2.1 *Sampling method*

The water and WC were sampled at Araromi, a coastal area in Ilaje Local Government Area (LGA) of Ondo State, Nigeria (Figure 1). The Ilaje community is an oil-producing area of Ondo State that shares boundaries with the Atlantic Ocean, Ogun, and Delta States. In June, water samples were collected from four water bodies, including the river (R) (6° 19' 55.195" N, 4° 29' 36.19" E), pond (P) (6° 19' 50.869" N, 4° 29' 40.265" E), estuary (E) (6° 19' 09.2" N, 4° 30' 28.1" E), and the sea (S) (6° 19' 26.106" N, 4° 29' 06.276" E), using pre-cleaned high-density polyethylene (HDPE) bottles. Five grab samples within 100 m of each other were taken from R, E, and S water sources, while grab samples from P were only 10 m apart due to the relatively small size of the water body. The sampling was carried out between 9 and 11 a.m. on the same day. The water samples from each location were aggregated and homogenized by gently shaking the bottles. Then, a representative sample was obtained from each aggregate for Fe content assessment and subsequent adsorption examinations. The WC was sourced locally from the bakery located in the sampling area, which also functions as a fish-smoking facility.

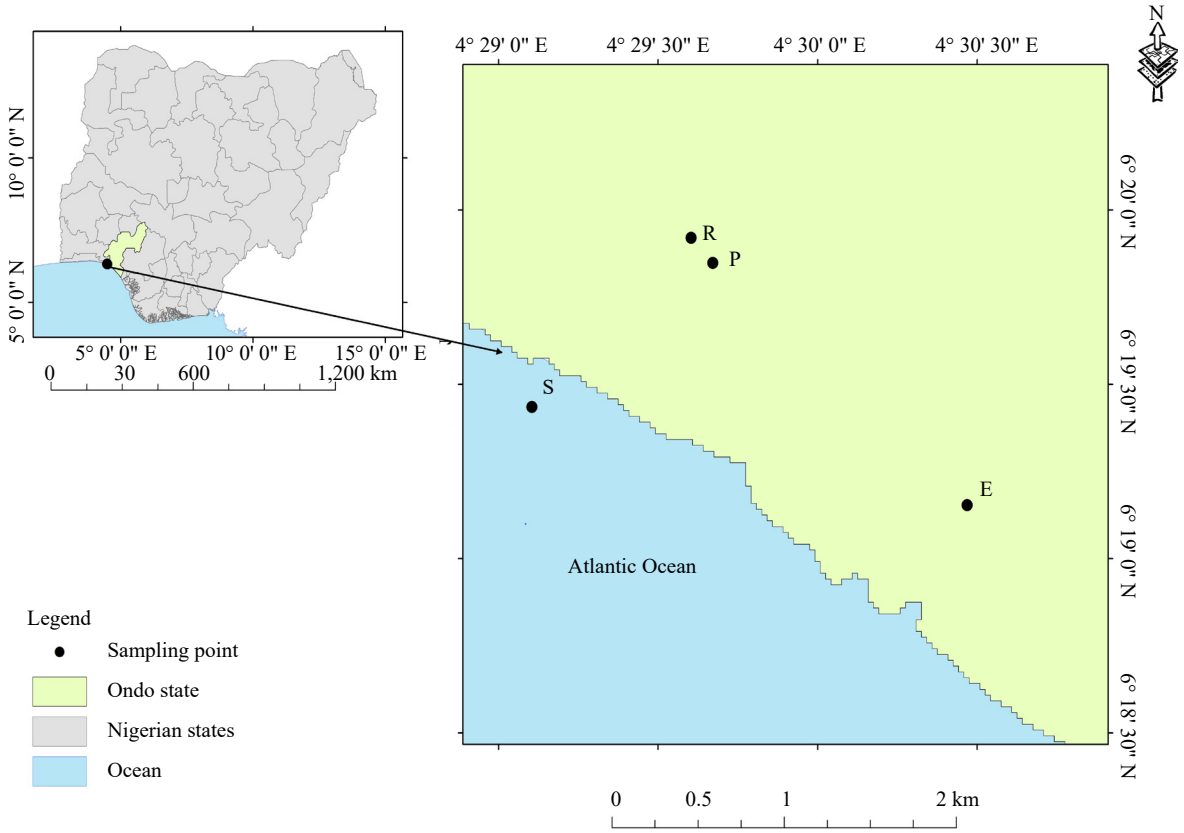

Figure 1. A map of the Ilaje Local Government Area, indicating the sampling locations

2.2 *Labware*

The glasswares used were beakers (500 mL), conical flasks (100 and 1000 mL), and volumetric flasks (1 L). A ceramic pestle and mortar, a magnetic stirrer-hot plate couple, a plastic funnel, a digital weighing balance, and a water distiller (Model WSB/4) were also included in the sample preparation kit. The consumables included Whatman No. 42 filter paper (6 µm mesh size) and nitric acid (70% purity). The physicochemical parameters (pH, salinity, temperature, total dissolved solids (TDS), electrical conductivity (EC), and dissolved oxygen (DO)) were monitored using a well-calibrated multi-parameter water analyzer (Hanna HI9819X Water Analyzer, USA).

2.3 *Preliminary study*

First, the background Fe concentrations of the water samples were determined using the standard procedure discussed in Section 2.4. By referring to the World Health Organization (WHO) standards, further adsorption studies were focused on samples that exceeded the Fe permissible limit of 0.3 mg/L.

2.4 *Fe analysis*

5 mL of 15.8 M nitric acid was added to 50 mL of the water sample in a pre-cleaned 100 mL conical flask to ensure complete mineralization and solubilization of the Fe content. The mixture was then heated to half its original volume on a hot plate (set to 90 °C) in the fume cupboard before being allowed to cool to room temperature. The digested sample was filtered into another 100 mL pre-cleaned conical flask using Whatman filter paper. The filtrate was diluted to mark with distilled water. An atomic absorption spectrophotometer (AAS, Buck Scientific VGP 210, USA) was used to measure the concentration of Fe.

2.5 *Adsorption study*

2.5.1 *Adsorbent pretreatment*

The WC was pre-cleaned by soaking for 5 min in 1 M HNO_3 (w/v = 10 g/mL). Then, it was thoroughly but gently rinsed in distilled water until the pH of the water reached 6.4. The charcoal was then oven-dried for 24 hours at 105 °C to remove residual minerals and moisture. Using a mortar and pestle, the dried WC was pounded. Then, it was sieved through a series of sieves with different mesh sizes to obtain regular-sized particles with diameters (dp) < 0.38 mm, 0.38 to 1.18 mm, and 1.18 to 2.00 mm. Henceforth, the WCs are referred to as 0.38dp, 1.18dp, and 2.00dp, respectively.

2.5.2 *Effect of adsorption conditions*

The individual effects of dosage, contact time, and temperature on WC's adsorption efficiency (ζ) against Fe were investigated for three particle sizes (0.38dp, 1.18dp, and 2.00dp).

i. Effect of adsorbent dosage

0.5, 1.0, 1.5, 2.0, and 3.0 g of WC were added to five different beakers containing 50 mL of seawater sample each, resulting in doses of 10, 20, 30, 40, and 60 g/L, respectively. The temperature was kept at 21 °C for 40 min with mild agitation. The mixture was then filtered to remove the impurities. AAS was used to determine Fe concentrations in the filtrate.

ii. Effect of contact time

In triplicates, 50 mL of the water sample was poured into 100 mL beaker samples at 21 °C. Approximately 2.0 g of each sample was added to the separate beakers (i.e., three prototypes) and gently agitated for 10 min. The procedure was repeated at 20, 30, 40, and 50 min contact times. In each case, the mixture was filtered and the amount of Fe concentration in the filtrates was determined.

iii. Effect of temperature

For each WC sample, approximately 2.0 g was placed in separate 100 mL beakers, each containing 50 mL of the water sample. The mixture was kept at approximately 20 °C on a magnetic stirrer. Other triplicates were carried out by ramping the temperature to 30, 40, 50, and 60 °C and holding it for the duration of the experiment before adding the adsorbent. For each sample, the mixture was filtered, and the concentration of Fe in the filtrate was determined accordingly.

2.5.3 *Estimation of sorption efficiency*

All of the experiments were carried out in batch mode. The sorption efficiency (i.e., the percentage of metal uptake by the sorbent, otherwise called percentage removal) was determined using Equation 1:

$$\zeta = \frac{C_0 - C_1}{C_0} \times 100\% \tag{1}$$

where C_0 and C_1 imply the Fe concentrations before and after adsorption, respectively.

Further, the WC adsorption capacity for Fe (q_e) was calculated using Equation 2:

$$q_e = \frac{C_0 - C_1}{m} \times V \tag{2}$$

where m is the mass of the WC (g) and V is the volume of the water sample (mL).

Quality assurance (QA) or quality control (QC): All analyses and calculations were done in triplicates at a probability level (p) = 0.05. All outliers were expunged before the mean of reliable triplicates was used as representative values.

2.6 *Modeling adsorption properties*

2.6.1 *Adsorption isotherms*

Adsorption isotherms describe the equilibrium between adsorbents and adsorbates at a particular temperature. The mechanism of Fe adsorption by WC was investigated using Langmuir and Freundlich isotherm models.

The Langmuir isotherm is one of the most widely used models. It proposes that adsorptions occur at specific (finite) homogeneous sites of the adsorbent in a monolayer pattern. The linearized form of the Langmuir equation is rendered as Equation 3:

$$\frac{C_e}{q_e} = \frac{C_0}{q_{max}} + \frac{1}{K_L q_{\max}} \tag{3}$$

where C_0 and C_e are the initial and equilibrium Fe concentrations (mg/L), q_e is the amount of Fe adsorbed per unit weight of WC at equilibrium (mg/g), K_L is the Langmuir constant (L/mg), and q_{max} is the maximum monolayer adsorption capacity (mg/g).

An essential factor of the Langmuir isotherm used to predict the favorability of the adsorption system is the separation factor, R_L, defined in Equation 4:

$$R_L = \frac{1}{1+K_L C_0} \tag{4}$$

where C_0 refers to the initial concentration of Fe (mg/L). In this context, the lower the value of R_L, the more favorable the adsorption. Specifically, adsorption is either unfavorable ($R_L > 1$), linear ($R_L = 1$), favorable ($0 < R_L < 1$), or irreversible ($R_L = 0$) [23,24].

The Freundlich model is an empirical model that allows for multi-layer adsorption on the adsorbent [25]. The linearized form of the Freundlich model, used in the current work, is expressed as Equation 5:

$$\ln q_e = \frac{\ln C_e}{n_F} + \ln K_F \tag{5}$$

where K_F is the equilibrium constant of adsorption and $1/n_F$ is the heterogeneity factor and the slope of the linearized form.

2.6.2 *Adsorption thermodynamics*

It is established that if the sorption capacity increases with temperature, the sorption process is endothermic, and the reverse implies exothermic adsorption [26]. The thermodynamic parameters (free energy (ΔG), enthalpy (ΔH), and entropy change (ΔS)) are determinable from the equilibrium constants of the Langmuir, Freundlich, or Temkin isotherm models, which determine the feasibility of the adsorption [27,28]. The thermodynamic parameters are derived using Equation 6:

$$\Delta G = RT \ln K_C \tag{6}$$

where R is the molar gas constant (8.314 J/mol.K), T is the adsorption temperature, and K_C is the equilibrium constant of adsorption. From the value of ΔG, another plot of ΔG against temperature (T) was used to determine ΔH and ΔS:

$$\Delta G = \Delta H - T\Delta S \tag{7}$$

2.6.3 *Adsorption kinetics*

By varying the contact time, the adsorption rate was modeled using Lagergren's first order and Ho's second-order equations [27,29]. The pseudo-first-order kinetic equation and the linearized form are given in Equation 8 and 9, respectively:

$$\frac{dq_t}{dt} = k_1(q_e - q_t) \tag{8}$$

$$\ln(q_e - q_t) = \ln q_e - k_1 t \tag{9}$$

where q_e and q_t are the amounts of Fe adsorbed (mg/g) at equilibrium and at time t (min), respectively, and k_1 is the rate constant (min^{-1}). The pseudo-first-order implies that the rate of adsorption change is directly proportional to the difference between the saturation concentration and the amount adsorbed per time [24,30]. In contrast, the pseudo-second-order model assumes that the rate-determining step is chemisorption (rather than physisorption) through the sharing or transfer of electrons at the adsorption interface. The pseudo-second-order kinetic equation used in the current study is given as Equation 10:

$$\frac{t}{q_t} = \frac{1}{k_2 q_e^2} + \frac{t}{q_e} \tag{10}$$

where k_2 is the rate constant (min^{-1}).

3. Results and discussion

3.1 *Status quo of Fe concentration*

Fe was undetectable in the R and P samples, but was found in the E and S samples at 0.17 and 0.55 mg/L, respectively. As a result, Fe levels in drinking water were found to be above the WHO permitted limit (i.e., 0.3 mg/L) only in the S sample [31]. The high Fe concentration in S is attributed to wrecked ships, abandoned vessels, indiscriminate disposal of waste metals from mechanic shops and scrap metals from industries, corroded jetty metalworks, corroded fishing hooks, and other metal-based anthropogenic activities. Hence, further Fe remediation and adsorption property analyses were based solely on the S sample.

3.2 *Effect of adsorption conditions*

Figure 2 depicts the influence of sorbent dosage, contact time, and temperature on the removal of Fe from S sample using WC with different particle sizes. The effect of dosage on Fe sorption efficiency of each particle size is illustrated in Figure 2(a). Regardless of particle size, an increase in Fe removal with adsorbent dosage was observed. Other studies have shown that increasing the amount of adsorbent gives additional surfaces for adsorption [32,33], therefore this result was expected. Irrespective of the dosage, the WC effectively lowers the Fe content in the seawater below the WHO standard limit for Fe in drinking water. As a result, the WC dosage of 10 g per 1 L of S was sufficient. The adsorption tendency also increases with the fineness of WC particles, i.e., the ζ (percentage removal) was in the order of 2.00dp < 1.18dp < 0.38dp. It implies that increasing the external surface area of WC enhances excess Fe removal from seawater due to the higher adsorption interface.

The influence of the contact time on the sorption efficiency of WC against Fe was also investigated. As depicted in Figure 2(b), Fe removal increases steadily with contact time for each particle size. Similarly, a steady and consistent

superiority in sorption efficiency was observed with a decrease in particle sizes. Likewise, as contact time increases, more adsorbates occupy the available adsorption sites provided by the enhanced external surface through WC pulverization. As a result, the adsorption tendency increases in the order of 2.00dp < 1.18dp < 0.38dp. Thus, the finer the particle size and the longer the contact time, the higher the Fe adsorption from the seawater.

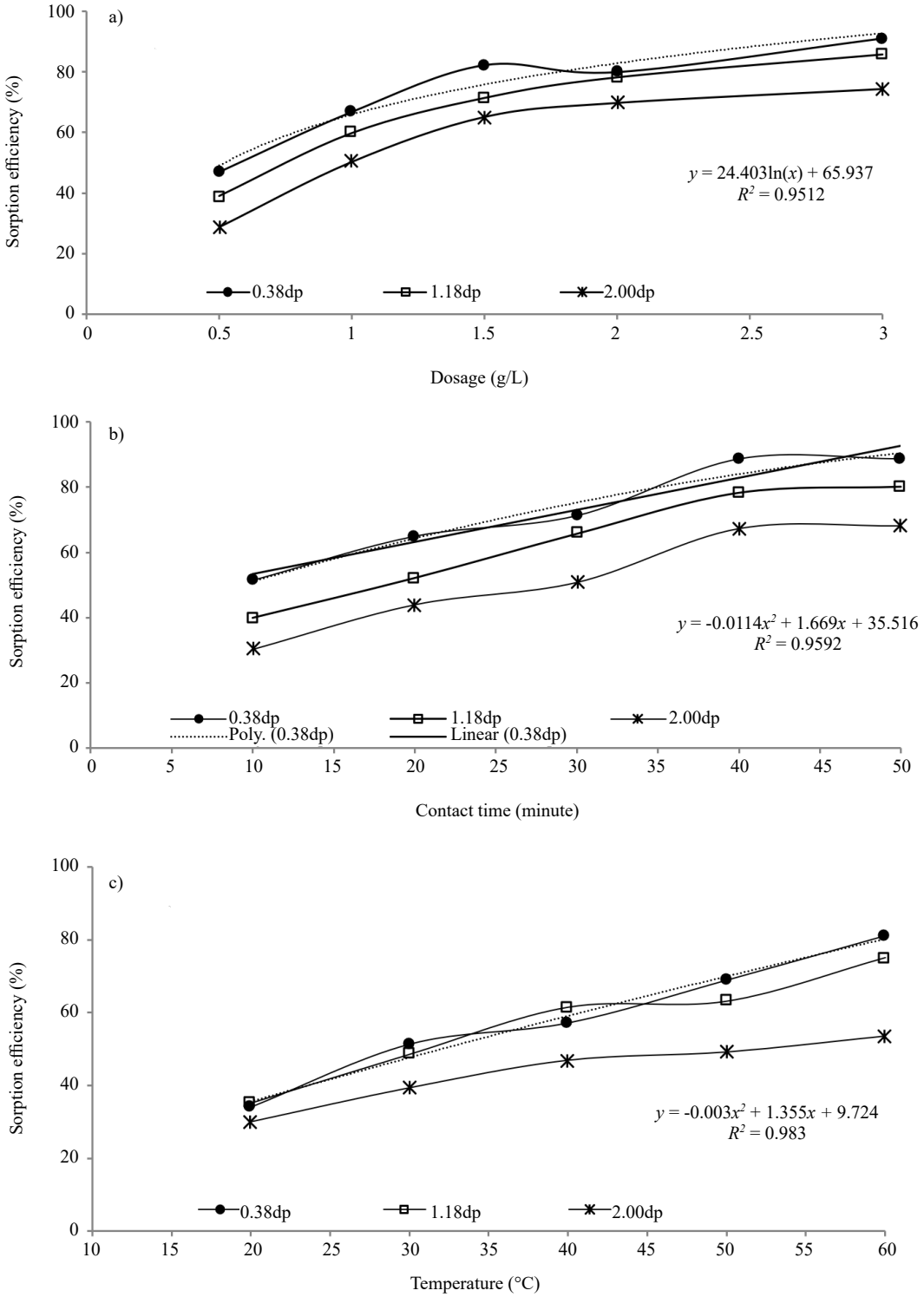

Figure 2. The effect of (a) dosage, (b) contact time, and (c) temperature on the sorption efficiency of WC

The effect of temperature on the efficiency of WC to remove excess Fe is depicted in Figure 2(c). A steady increase in Fe adsorbed by WC with temperature was observed, inferring the predominance of endothermic adsorption. The distinction between the effects of temperature on the adsorption of 1.18dp and 0.38dp WC was indistinct, compared with that of 2.00dp WC. The observed non-linear relationship between particle size and adsorption temperature is attributed to the adsorption thermodynamics because the adsorption-desorption equilibrium was altered by temperature change. However, with larger particles (lesser surface area), the adsorption haphazardness lessened as the adsorption equilibrium was reached faster and more straightforward on the fewer active sites available.

Assuming the experiments were error-free, we modeled the adsorption data for each condition (with 0.38dp WC as the most favorable sample) to identify when 100% sorption efficiency could be attained (Figure 2). Respectively, we found the best fits for dosage, contact time, and temperature to be logarithmic, polymeric, and polymeric. Therefore, for $\zeta = 100\%$, the dosage, contact time, and temperature should be 4.04 g/L, 56.0 min, and 81.2 °C, respectively.

The respective adsorption properties (isotherm, kinetics, and thermodynamics) were investigated using established models to better understand the adsorption mechanism, rate, and feasibility.

3.3 *Adsorption properties*

3.3.1 *Isotherm*

The fitting of the experimental adsorption data to Langmuir and Freundlich isotherm models is provided in Figure 3, while the deduced parameters, degree of fitness (by R^2), and model equations are listed in Table 1. For both models, the degree of fitness was highest and lowest at 1.18dp and 2.00dp, respectively. However, since the R_L was generally < 1, the adsorption was favorable, i.e., monolayer surface adsorption was predominant. However, the Freundlich model also shows $1/n_F < 1$, hence the adsorption is favorable [34]. Additionally, the K_F values indicate that the amount of Fe adsorbed by WC follows the trend of 0.38dp > 1.18dp > 2.00dp. This trend indicates that 0.38dp WC has the highest Fe adsorption capacity [35,36]. A similar result was observed for the q_{max} through the Langmuir model, showing that the 0.38dp-sized WC exhibited the highest values among the other WC samples. The least n_F value recorded by the 2.00dp indicated that the WC surface was more heterogeneous than that of other particle sizes [37]. This observation buttressed the axiom that adsorption surfaces become more heterogeneous as the n_F value approaches zero [38]. Thus, given that $1/n_F < 1$, the adsorption is likely to be chemisorption. Since the Freundlich model generally evinced a better fit than the Langmuir model (i.e., superior R^2 values), we infer that Fe collection on the WC granules was predominantly multidimensional rather than a monolayer phenomenon. The high R^2 value of the 1.18dp Freundlich models might result from intraparticle diffusion occurring in a chemisorption-predominant removal. If the adsorption process were strictly monolayer, the degree of fitness would have been directly proportional to particle fineness. However, because intraparticle diffusion into the available pore probably ensued, Fe multi-layer adsorption occurred, thereby favoring the Freundlich model. Another possibility for the heterogeneous active sites on the surface of the charcoal could be the presence of various surface oxygen functionalities tethered during its formation from wood-burning (dry oxidation) as well as by the wet (nitric) acid during sample pretreatment [39,40]. Dry and wet oxidations have been attributed to the formation of various acid and basic oxygen functionalities [41].

Table 1. Adsorption isotherm parameters for adsorption of Fe in seawater by WC

Sample	Langmuir					Freundlich				
	q_{max} (mg/g)	K_L (L/mg)	R_L	R^2	Model equation	K_F (m/mg)	n_F	$1/n_F$	R^2	Model equation
0.38dp	0.0474	3.713	0.328	0.699	y = 21.09x + 5.68	0.0534	1.608	0.622	0.898	y = 0.622x – 2.93
1.18dp	0.0455	2.621	0.409	0.994	y = 22.02x + 8.40	0.0459	1.459	0.686	0.999	y = 0.686x – 3.08
2.00dp	0.0405	1.772	0.505	0.558	y = 24.72x + 13.9	0.0345	1.350	0.741	0.846	y = 0.741x – 3.37

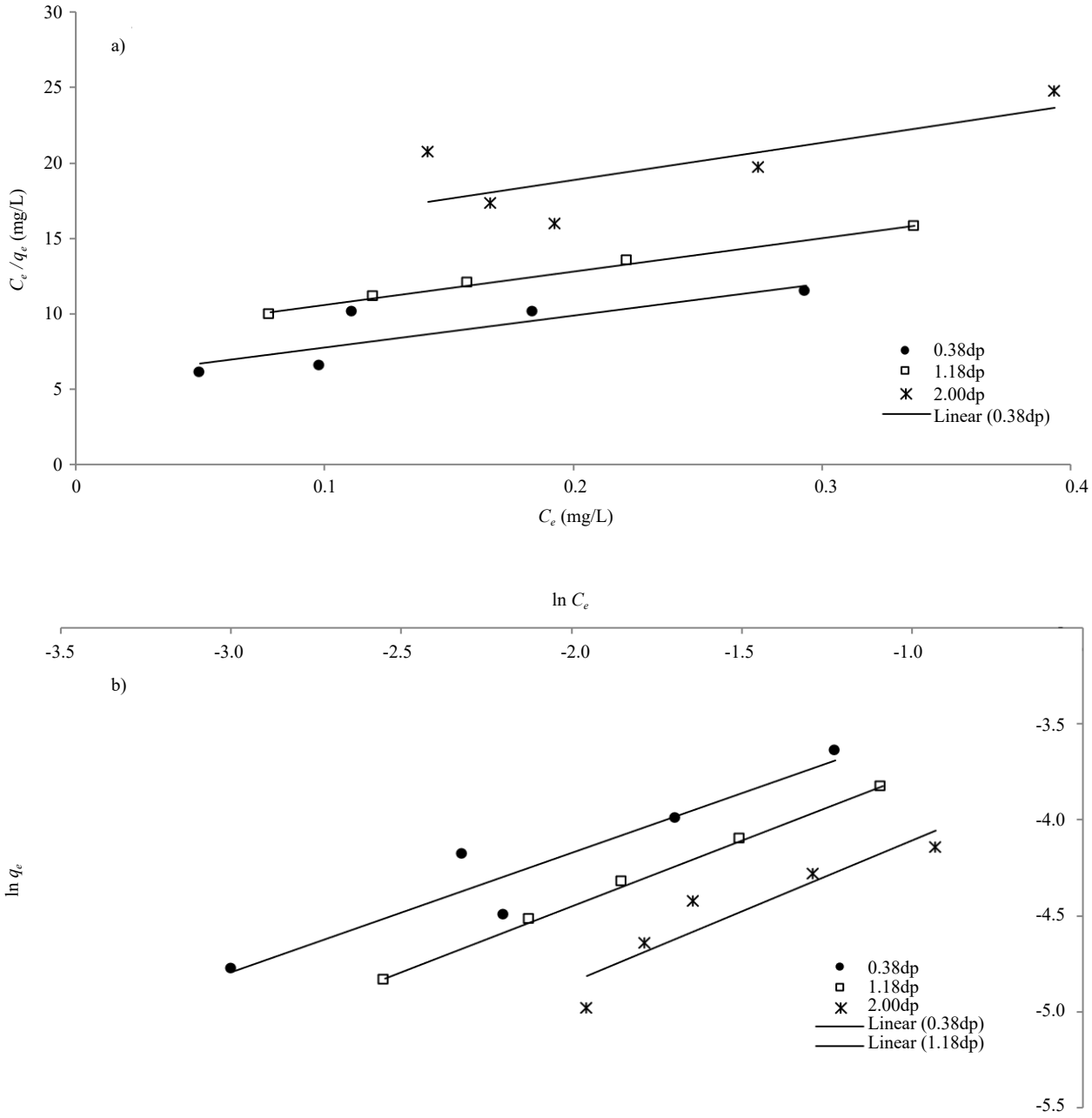

Figure 3. (a) Langmuir and (b) Freundlich models for the adsorption of Fe on WC

3.3.2 *Kinetics*

Using the experimental data of Fe adsorption under various contact times (Section 2.6.3), the adsorption rate was fitted with pseudo-first-order and pseudo-second-order models as depicted in Figure 4. The derived parameters and models are provided in Table 2. The linearity of all the plots shows that the Fe removal mechanism was via physical and chemical adsorption [24,42]. Except for the 0.38dp WC, the pseudo-second-order kinetic model outperformed the pseudo-first-order model in terms of degree of fitness. Our findings indicate that the pseudo-first-order model provided a good fit when the adsorbate collected on the adsorbent was low, as given by the q_1 value of 0.0074 in Table 2 [43]. Thus, the pseudo-first-order model best explains the adsorption kinetics for the 0.38dp WC, while the pseudo-second-order model is more suitable to predict the kinetics for the 1.18dp and 2.00dp WC. Also, the rate constant of pseudo-second-

order adsorption (k_2) was significantly higher than that obtained for the pseudo-first-order model. This observation showed a slower uptake of Fe^{2+} onto the WC [15,44]. The pseudo-second-order model also showed little difference in q_2 and q for the 0.38dp and 1.18dp WC compared to q_1 of the pseudo-first-order model. Therefore, the rate-determining step may stem from the chemical adsorption, which involves valence forces via electron sharing or exchange at the adsorption interface [17,45].

Table 2. Adsorption kinetics parameters for adsorption of Fe in seawater by WC

Sample	q (mg/g)	Pseudo-first-order				Pseudo-second-order			
		q_1 (mg/g)	k_1 (min^{-1})	R^2	Model equation	q_2 (mg/g)	k_2 (min^{-1})	R^2	Model equation
0.38dp	0.0123	0.00737	0.038	0.989	y = – 0.038x – 4.91	0.0157	4.55	0.974	y = 63.8x + 893
1.18dp	0.0111	0.0216	0.099	0.864	y = – 0.099x – 3.84	0.0159	2.99	0.978	y = 63.1x + 1331
2.00dp	0.0094	0.0117	0.067	0.946	y = – 0.067x – 4.45	0.0140	2.83	0.992	y = 71.3x + 1193

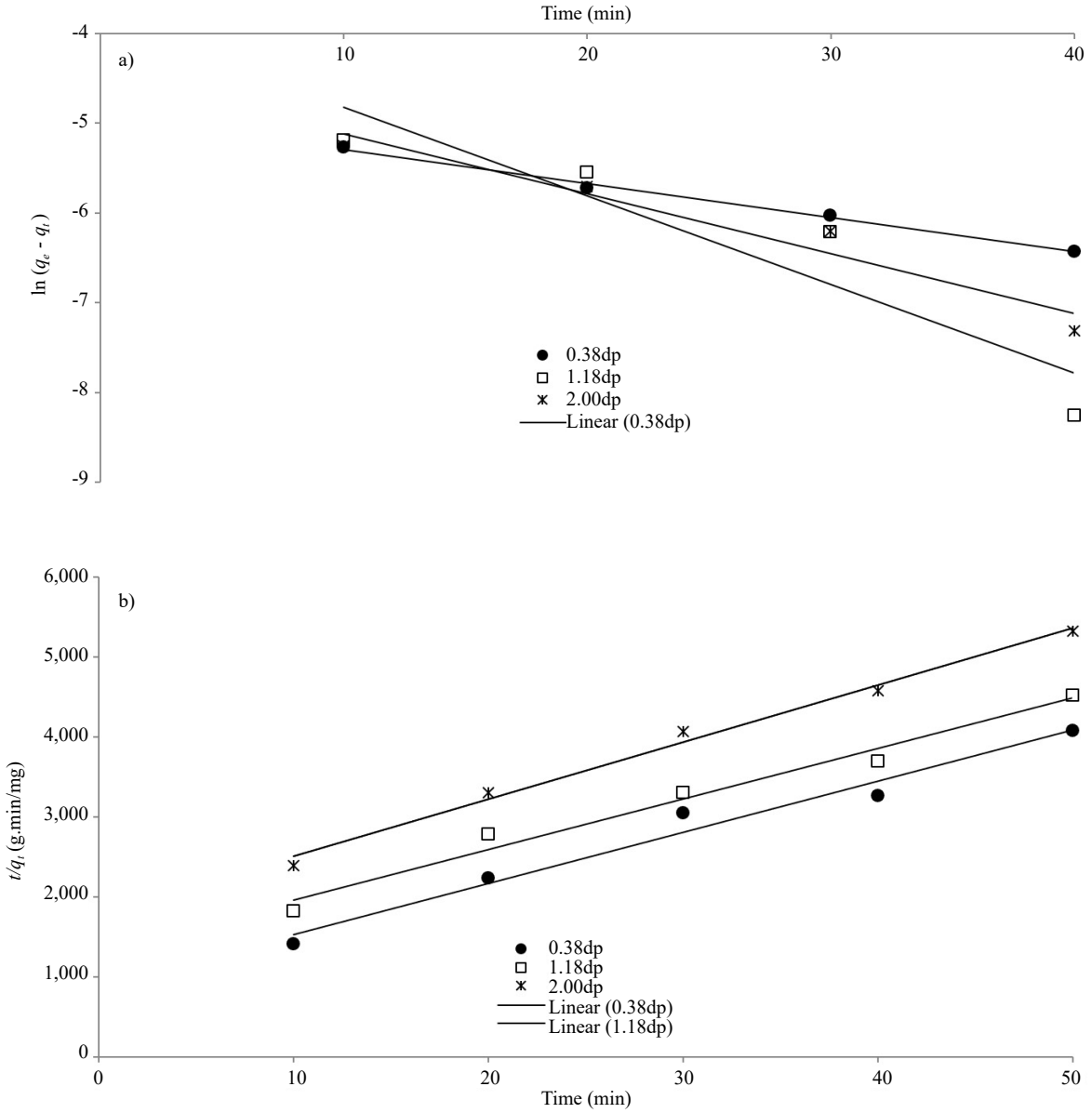

Figure 4. (a) Pseudo-first-order and (b) pseudo-second-order kinetic models for the adsorption of Fe on WC

3.3.3 *Thermodynamics*

The influence of temperature on the Fe adsorption on WC provides the basis for the thermodynamic study. We observed that Fe removal increased with temperature, implying an endothermic process. The increased entropy of Fe ions at elevated temperatures seems to facilitate intraparticle diffusion of the adsorbate onto the adsorbent's external surface and inner pore walls [46]. From Equation 6, the ΔS and ΔH are obtained as the slope and intercept, respectively. Based on the plots in Figure 5, we obtained the respective entropies (99.2, 74.3, and 28.1 J/mol) and heat contents (-39.5, -32.1, and -19.0 kJ/mol) of Fe adsorption by 0.38dp, 1.18dp, and 2.00dp WC (Table 3).

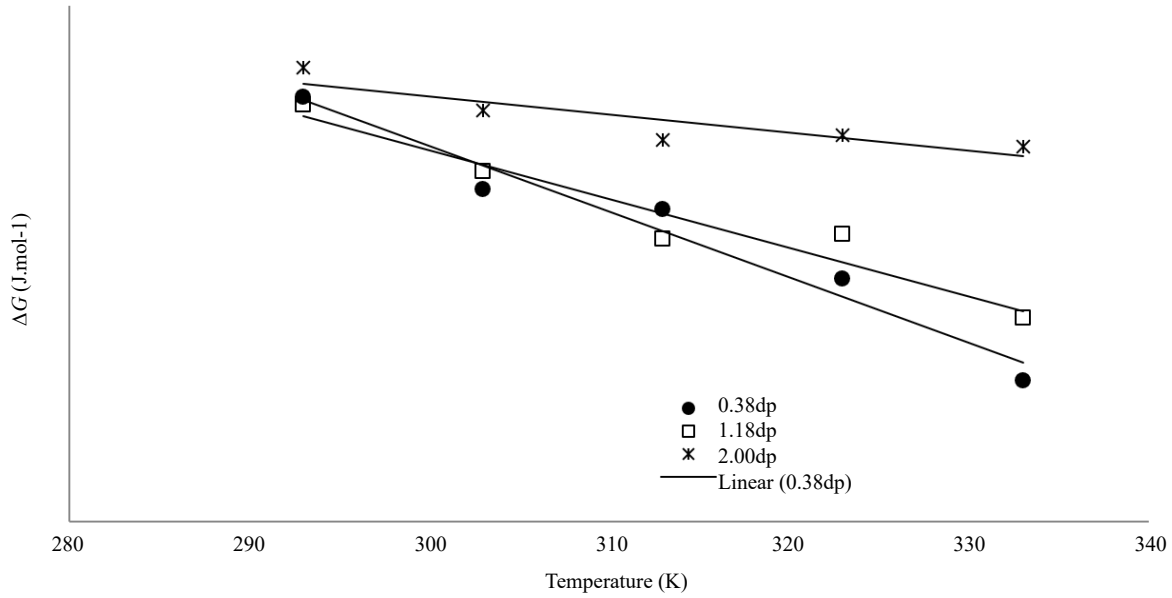

Figure 5. Thermodynamic plot for (a) 0.38dp, (b) 1.18dp, and (c) 2.00dp WCs adsorption of Fe

Table 3. Adsorption thermodynamics parameters for adsorption of Fe in seawater by WC

Sample	ΔG~T				Gibbs free energy, ΔG (kJ/mol)				
	ΔH (kJ/mg)	ΔS (kJ/mg.K)	R^2	Model equation	293	303	313	323	333
0.38dp	40.47	102.1	0.962	y = – 0.102x + 40.5	– 10.4	– 9.44	– 8.45	– 7.46	– 6.47
1.18dp	32.50	75.79	0.935	y = – 0.076x + 32.5	– 10.3	– 9.54	– 8.80	– 8.06	– 7.31
2.00dp	19.05	28.17	0.799	y = – 0.028x + 19.0	– 10.8	– 10.5	– 10.2	– 9.95	– 9.67

Adsorptions are classified into physisorption, physi-chemisorption, and chemisorption based on the ΔH values of ranges 2 to 20 kJ/mol, 20 to 40 kJ/mol, and > 40 kJ/mol, respectively [34,47]. In the current study, it is observed that Fe collection on the WC surfaces fell within the physi-chemisorption, inferring the relative fitness of the Langmuir isotherm despite a better fit with Freundlich. Also, the prevalence of chemisorption increased with pulverization, which is attributed to an increase in the availability of O-bearing chemical functionalities on the inner structure of the adsorbent [40,48]. Similarly, the randomness of Fe distribution, indicated by the ΔS, also increased with the external surface area provided by pulverization, as the negative values of ΔG confirm the feasibility and spontaneity of the adsorption [24,48].

Regarding the adsorption properties, the sorption observed was predominantly multi-layer. The adsorption sites also exhibited different affinities based on the superior correlation coefficients of Freundlich over Langmuir. Besides, the adsorption favors the pseudo-second-order model over the pseudo-first-order model, thereby confirming the

predominance of chemisorption over physisorption [47]. Finally, the adsorption thermodynamic values determined the feasibility of the adsorption and confirmed that the process was spontaneous and endothermic. Therefore, the successful modeling of Fe removal by WC enables a reliable and large-scale use.

3.4 *Effect of WC particle size on the physicochemical properties of treated S samples*

After establishing the efficacy of WC to adsorb Fe from seawater, this study further assessed the implications of the removal on the relevant physicochemical properties of the seawater (Table 4). Except for pH and DO (initially within the permissible range but improved), WC moderated most physicochemical properties to the permissible standard range for drinking water set by the WHO/Nigerian Industrial Standard (NIS) [31,49,50]. However, the salinity levels were still in the non-tolerable range (> 0.9 ppt). We opine that the sorbent requires increased dosage or surface chemical treatment to achieve an efficient and simultaneous salinity reduction. Significant to this study is the influence of the particle size of the sorbent on TDS removal, DO elevation, showing negative and high oxidation-reduction potential (ORP), and turbidity reduction. As initially observed with excess Fe removal, the finer the particles, the more efficient the overall purification.

Table 4. Physicochemical properties of seawater (S) upon contact with various WC particle sizes

Parameter	Raw S sample	0.38dp - treated	1.18dp - treated	2.00dp - treated	WHO/NIS standard
pH	7.85	6.88	6.95	6.98	6.5 – 8.5
Conductivity (µS/cm)	39,980	2,330	2,700	3,140	2,500
TDS (ppm)	19,990	8,570	10,140	11,180	1,000/500
Salinity (ppt)	26.18	5.280	6.428	6.840	< 0.6 (good) 0.6 – 0.9 (fair) 0.9 – 1.2 (poor) > 1.2 (hazardous)
Turbidity (NTU)	122	2.85	4.25	5.64	1 – 5
ORP (mV)	24.6	-38.1	-28.66	-28.56	-50
DO (mg/L)	6.31	8.14	7.80	7.88	≥ 5

4. Conclusion

Due to the lack of potable water and water purification technology for residents of the Araromi coastal regions of Nigeria, we were prompted to investigate the feasibility of using readily available wood-based charcoal to lower the Fe content of their neighboring seawater to the WHO standard for drinking water. Based on different particle sizes, the sorption efficiency and adsorption properties were studied in detail. We observed that the finer the particle size, the more efficient the adsorption was, with Fe removal efficiency of 90.9%, 85.8%, and 74.4% for particle sizes of 0.38dp, 1.18dp, and 2.00dp with 3 g/L dosages after 50 min of contact at room temperature. The sorption efficiency increased with dosage, contact time, and temperature, and was optimized at 4.04 g/L, 56.0 min, and 81.2 °C, respectively.

Adsorption modeling showed the favorability of Fe adsorption via Freundlich over Langmuir isotherms, suggesting the presence of various active adsorption sites, intraparticle diffusion, and multi-layer adsorption. Kinetically, the pseudo-second-order model was more suitable for describing the Fe adsorption on the charcoal, providing information on the prevalence of chemical reaction at the adsorption interface. The thermodynamics study also confirms the endothermic process of the adsorption as the ΔH, ΔS, and ΔG values evinced physi-chemisorption, spontaneity, and feasibility, respectively. Overall, the finer the particle size, the better the Fe adsorption. Therefore, we conclude that the supposedly locally-sourced waste wood-based charcoal could efficiently remove the Fe content of seawater to a potable level. Before oral consumption of the treated water can be recommended, additional studies are required to improve the efficiency of the adsorbent via physical activation (rather than chemical activation), confirm other trace metals that may co-adsorb with Fe, and test the quality of the treated water for pollutants that may have eluted from the untreated charcoal. The last two suggestions are limitations of the current studies.

Acknowledgement

The authors appreciate the moral support of our colleague, Usman Hassan.

Conflict of interest

The authors declare no conflict of interest.

References

[1] Sheng JJ, Wang XP, Gong P, Tian LD, Yao TD. Heavy Metals of the Tibetan Top Soils Level, Source, Spatial Distribution, Temporal Variation and Risk Assessment. *Environmental Science and Pollution Research*. 2012; 19: 3362-3370. Available from: doi:10.1007/s11356-012-0857-5.

[2] Yan Y, Han L, Yu R, Hu GR, Zhang WF, Cui JY, et al. Background Determination, Pollution Assessment and Source Analysis of Heavy Metals in Estuarine Sediments from Quanzhou Bay, Southeast China. *Catena*. 2020; 187: 104322. Available from: doi:10.1016/j.catena.2019.104322.

[3] Singh D, Tiwari A, Gupta R. Phytoremediation of Lead from Wastewater Using Aquatic Plants. *Journal of Agricultural Technology.* 2012; 8(1): 1-11. Available from: doi:10.7439/ijbr.v2i7.124.

[4] Peña-Fernández A, González-Muñoz MJ, Lobo-Bedmar MC. Establishing the Importance of Human Health Risk Assessment for Metals and Metalloids in Urban Environments. *Environment International*. 2014; 72: 176-185. Available from: doi:10.1016/j.envint.2014.04.007.

[5] Von Haehling S, Ebner N, Evertz R, Ponikowski P, Anker SD. Iron Deficiency in Heart Failure. *JACC: Heart Failure*. 2019; 7: 36-46. Available from: doi:10.1016/j.jchf.2018.07.015.

[6] Schweitzer PA. *Corrosion and Corrosion Protection Handbook*. 2nd ed. New York: Routledge; 1989. Available from: doi:10.1201/9781315140384.

[7] Kim JS, Zhang L, Keane MA. Removal of Iron from Aqueous Solutions by Ion Exchange with Na-Y Zeolite. *Separation Science and Technology*. 2001; 36(7): 1509-1525. Available from: doi:10.1081/SS-100103885.

[8] Ghosh D, Solanki H, Purkait MK. Removal of Fe (II) from Tap Water by Electrocoagulation Technique. *Journal of Hazardous Material*. 2008; 155(1-2): 135-143. Available from: doi:10.1016/j.jhazmat.2007.11.042.

[9] Alguacil FJ, Lopez FA. Separation Iron (III)-Manganese (II) via Supported Liquid Membrane Technology in the Treatment of Spent Alkaline Batteries. *Membranes*. 2021; 11(12): 991. Available from: doi:10.3390/membranes11120991.

[10] Aly AM, Kamel MM, Hamdy A, Mohammed KZ, Abbas MA. Reverse Osmosis Pretreatment: Removal of Iron in Groundwater Desalination Plant in Shupramant-Giza – A Case Study. *Current World Environment*. 2012; 7(1): 23-32. Available from: doi:10.12944/CWE.7.1.04.

[11] Ali MBS, Ennigrou DJ, Hamrouni B. Iron Removal from Brackish Water by Electrodialysis. *Environmental Technology*. 2013; 34(17): 2521-2529. Available from: doi:10.1080/09593330.2013.777081.

[12] Hu G, Wu Y, Chen D, Wang Y, Qi T, Wang L. Selective Removal of Iron (III) from Highly Salted Chloride Acidic Solutions by Solvent Extraction using Di (2-ethylhexyl) Phosphate. *Frontiers of Chemical Science and Engineering*. 2020; 15: 528-537. Available from: doi:10.1007/s11705-020-1955-4.

[13] Jinal HN, Gopi K, Prittesh P, Prittesh P, Kartik VP, Amaresan N. Phytoextraction of Iron from Contaminated Soils by Inoculation of Iron-Tolerant Plant Growth-Promoting Bacteria in Brassica juncea L. Czern. *Environmental Science and Pollution Research*. 2019; 26(32): 32815-32823. Available from: doi:10.1007/s11356-019-06394-2.

[14] Tang X, Qiao J, Wang J, Huang K, Guo Y, Xu D, et al. Bio-Cake Layer Based Ultrafiltration in Treating Iron- and Manganese-Containing Groundwater: Fast Ripening and Shock Loading. *Chemosphere*. 2021; 268: 128842. Available from: doi:10.1016/j.chemosphere.2020.128842.

[15] Dim PE, Mustapha LS, Termtanum M, Okafor JO. Adsorption of Chromium (VI) and Iron (III) Ions onto Acid-Modified Kaolinite: Isotherm, Kinetics and Thermodynamics Studies. *Arabian Journal of Chemistry*. 2021; 14(4): 103064. Available from: doi:10.1016/j.arabjc.2021.103064.

[16] Gunatilake S. Methods of Removing Heavy Metals from Industrial Wastewater. *Journal of Multidisciplinary Engineering Science Studies*. 2015; 1(1): 12-18. Available from: https://www.researchgate.net/publication/287818349_Methods_of_Removing_Heavy_Metals_from_Industrial_Wastewate [Accessed 14th

February 2021].
[17] Zhang X, Hao Y, Wang X, Chen Z. Adsorption of Iron (III), Cobalt (II), and Nickel (II) on Activated Carbon Derived from Xanthoceras Sorbifolia Bunge Hull: Mechanisms, Kinetics and Influencing Parameters. *Water Science and Technology*. 2017; 75(8): 1849-1861. Available from: doi:10.2166/wst.2017.067.
[18] Baruah BK, Das B, Haque A, Misra K, Misra AK. Iron Removal Efficiency of Different Bamboo Charcoals: A Study on Modified Indigenous Water Filtration Technique in Rural Areas of Assam. *Journal of Chemical and Pharmaceutical Research*. 2011; 3(2): 454-459. Available from: https://www.researchgate.net/publication/286111725_Iron_removal_efficiency_of_different_bamboo_charcoals_A_study_on_modified_indigenous_water_filtration_technique_in_rural_areas_of_Assam [Accessed 6th March 2021].
[19] Aji MM, Gutti B, Highina BK. Application of Activated Carbon in Removal of Iron and Manganese from Alau Dam Water in Maiduguri. *Columban Journal of Life Science*. 2015; 17(1): 35-39. Available from: https://www.researchgate.net/profile/Mohammed-Aji/publication/304404245_APPLICATION_OF_ACTIVATED_CARBON_IN_REMOVAL_OF_IRON_AND_MANGANESE_FROM_ALAU_DAM_WATER_IN_MAIDUGURI/links/576e8df608ae842225a88077/APPLICATION-OF-ACTIVATED-CARBON-IN-REMOVAL-OF-IRON-AND-MANGANESE-FROM-ALAU-DAM-WATER-IN-MAIDUGURI.pdf [Accessed 19th November 2020].
[20] Goher ME, Hassan AM, Abdel-Moniem IA, Fahmy AH, Abdo MH, El-Sayed SM. Removal of Aluminium, Iron and Manganese Ions from Industrial Wastes using Granular Activated Carbon and Amberlite IR-120H. *The Egyptian Journal of Aquatic Research*. 2015; 41(2): 155-164. Available from: doi:10.1016/j.ejar.2015.04.002.
[21] Das B, Hazarika P, Saikia G, Kalita H, Goswani DC, Das HB, et al. Removal of Iron from Groundwater by Ash: A Systematic Study of a Traditional Method. *Journal of Hazardous Material*. 2007; 141(3): 834-841. Available from: doi:10.1016/j.jhazmat.2006.07.052.
[22] Renu MA, Singh K. Heavy Metal Removal from Wastewater using Various Adsorbents: A Review. *Journal of Water Reuse and Desalination*. 2017; 7(4): 387-419. Available from: doi:10.2166/wrd.2016.104.
[23] Foo KY, Hameed BH. Insights into The Modeling of Adsorption Isotherm Systems. *Chemical Engineering Journal*. 2010; 156: 2-10. Available from: doi:10.1016/j.cej.2009.09.013.
[24] Edet UA, Ifelebuegu AO. Kinetics, Isotherms, and Thermodynamic Modeling of the Adsorption of Phosphates from Model Wastewater using Recycled Brick Waste. *Processes*. 2020; 8: 665. Available from: doi:10.3390/pr8060665.
[25] Diraki A, Mackey HR, McKay G, Abdala A. Removal of Emulsified and Dissolved Diesel Oil from High Salinity Wastewater by Adsorption onto Graphene Oxide. *Journal of Environmental Chemical Engineering*. 2019; 7(3): 103106. Available from: doi:10.1016/j.jece.2019.103106.
[26] Mustapha S, Shuaib DT, Ndamitso MM, Etsuyankpa MB, Sumaila A, Mohammed UM, et al. Adsorption Isotherm, Kinetic and Thermodynamic Studies for the Removal of Pb (II), Cd (II), Zn (II) and Cu (II) Ions from Aqueous Solutions using Albizia Lebbeck Pods. *Applied Water Science*. 2019; 9(6): 1-11. Available from: doi:10.1007/s13201-019-1021-x.
[27] Gunorubon AJ, Chukwunonso N. Kinetics, Equilibrium and Thermodynamics Studies of Fe^{3+} Ion Removal from Aqueous Solutions using Periwinkle Shell Activated Carbon. *Advances in Chemical Engineering and Science*. 2018; 8(2): 82004. Available from: doi:10.4236/aces.2018.82004.
[28] Salehzadeh J. Removal of Heavy Metals Pb^{2+}, Cu^{2+}, Zn^{2+}, Cd^{2+}, Ni^{2+}, Co^{2+} and Fe^{3+} from Aqueous Solutions by using Xanthium Pensylvanicum. *Leonardo Journal of Sciences*. 2013; 23: 97-104. Available from: http://ljs.academicdirect.org/A23/097_104.htm [Accessed 15th March 2021].
[29] Wang N, Xu X, Li H, Zhai J, Yuan L, Zhang K, Yu H. Preparation and Application of a Xanthate-modified Thiourea Chitosan Sponge for the Removal of Pb (II) from Aqueous Solutions. *Industrial & Engineering Chemistry Research*. 2016; 55(17): 4960-4968. Available from: doi:10.1021/acs.iecr.6b00694.
[30] Simonin JP. On the Comparison of Pseudo-First Order and Pseudo-Second Order Rate Laws in the Modeling of Adsorption Kinetics. *Chemical Engineering Journa*l. 2016; 300: 254-263. Available from: doi:10.1016/j.cej.2016.04.079.
[31] World Health Organisation (WHO). *Guidelines for Drinking-Water Quality: Fourth Edition Incorporating the First Addendum*. Geneva: World Health Organization; 2017. Available from: https://www.who.int/publications/i/item/9789241549950 [Accessed 9th April 2021].
[32] Ali RM, Hamad HA, Hussein MM, Malash GF. Potential of using Green Adsorbent of Heavy Metal Removal from Aqueous Solutions: Adsorption Kinetics, Isotherm, Thermodynamic, Mechanism and Economic Analysis. *Ecological Engineering*. 2016; 91: 317-332. Available from: doi:10.1016/j.ecoleng.2016.03.015.
[33] Rafati L, Ehrampoush MH, Rafati AA, Mokhtari M, Mahvi AH. Modeling of Adsorption Kinetic and Equilibrium

Isotherms of Naproxen onto Functionalized Nano-Clay Composite Adsorbent. *Journal of Molecular Liquids*. 2016; 224: 832-841. Available from: doi:10.1016/j.molliq.2016.10.059.
[34] Cheruiyot GK, Wanyonyi WC, Kiplimo JJ, Maina EN. Adsorption of Toxic Crystal Violet Dye using Coffee Husks: Equilibrium, Kinetics and Thermodynamics Study. *Scientific African*. 2019; 5: e00116. Available from: doi:10.1016/j.sciaf.2019.e00116.
[35] Kumar PS, Korving L, Keesman KJ, van Loosdrecht MCM, Witkamp G-J. Effect of Pore Size Distribution and Particle Size of Porous Metal Oxides on Phosphate Adsorption Capacity and Kinetics. *Chemical Engineering Journal*. 2019; 358: 160-169. Available from: doi:10.1016/j.cej.2018.09.202
[36] Bao Y, Yuan F, Zhao X, Liu Q, Gao Y. Equilibrium and Kinetic Studies on the Adsorption Debittering Process of Ponkan (Citrus Retriculata Blanco) Juice using Macroporous Resins. *Food and Bioproducts Processing*. 2015; 94: 199-207. Available from: doi:10.1016/j.fbp.2013.12.009.
[37] Ayawei N, Ebelegi AN, Wankasi D. Modelling and Interpretation of Adsorption Isotherms. *Journal of Chemistry*. 2017; 3039817. Available from: doi:10.1155/2017/3039817.
[38] Kumar V, Srinivas G, Wood B, Ramisetty KK, Stewart AA, Howard CA, et al. Characterization of Adsorption Site Energies and Heterogeneous Surfaces of Porous Materials. *Journal of Materials Chemistry A*. 2019; 7(17): 10104-10137. Available from: doi:10.1039/C9TA00287A.
[39] Petrovic B, Gorbounov M, Soltani SM. Influence of Surface Modification on Selective CO^2 Adsorption: A Technical Review on Mechanisms and Methods. *Microporous and Mesoporous Materials*. 2021; 312: 110751. Available from: doi:10.1016/j.micromeso.2020.110751.
[40] Adelodun AA, Kim K-H, Ngila JC, Szulejko J. A Review on the Effect of Amination Pretreatment for the Selective Separation of CO_2. *Applied Energy*. 2015; 158: 631-642. Available from: doi:10.1016/j.apenergy.2015.08.107.
[41] Abegunde SM, Idowu KS, Adejuwon OM, Adeyemi-Adejolu T. A Review on the Influence of Chemical Modification on the Performance of Adsorbents. *Resources, Environment and Sustainability*. 2020; 1: 100001. Available from: doi:10.1016/j.resenv.2020.100001.
[42] Huang JH, Deng RJ, Huang KL. Equilibria and Kinetics of Phenol Adsorption on a Tolene-Modified Hyper-Cross-Linked Poly (Styrene-Co-Divinylbenzene) Resin. *Chemical Engineering Journal*. 2011; 171(3): 951-957. Available from: doi:10.1016/j.cej.2011.04.045.
[43] Song G, Zhu XZ, Liao Q, Ding YD, Chen L. An Investigation of CO_2 Adsorption Kinetics on Porous Magnesium Oxide. *Chemical Engineering Journal*. 2016; 283: 175-183. Available from: doi:10.1016/j.cej.2015.07.055.
[44] Chen DZ, Zhang JX, Chen JM. Adsorption of Methyl Tert-Butyl Ether using Granular Activated Carbon Equilibrium and Kinetic Analysis. *International Journal of Environmental Science and Technology*. 2011; 7(2): 235-242. Available from: doi:10.1007/BF03326133.
[45] Vasiliu S, Bunia I, Racovita S, Neagu V. Adsorption of Cefotaxime Sodium Salt on Polymer Coated Ion Exchange Resin Microparticles: Kinetics, Equilibrium and Thermodynamic Studies. *Carbohydrate Polymer*. 2011; 85(2): 376-387. Available from: doi:10.1016/j.carbpol.2011.02.039.
[46] Coskun YI, Aksuner N, Yanik J. Sandpaper Wastes as Adsorbent for the Removal of Brilliant Green and Malachite Green Dye. *Acta Chimica Slovenica*. 2019; 66(2): 402-413. Available from: doi:10.17344/acsi.2018.4881.
[47] Ding L, Deng HP, Wu C, Han X. Affecting Factors, Equilibrium, Kinetics and Thermodynamics of Bromide Removal from Aqueous Solutions by MIEX Resin. *Chemical Engineering Journal*. 2012; 181: 360-370. Available from: doi:10.1016/j.cej.2011.11.096.
[48] Adelodun AA, Ngila JC, Kim D-G, Jo Y-M. Isotherm, Thermodynamic and Kinetic Studies of Selective CO_2 Adsorption on Chemically Modified Carbon Surfaces. *Aerosol and Air Quality Research*. 2016; 16: 3312-3329. Available from: doi:10.4209/aaqr.2016.01.0014.
[49] Adamu IH, Mubarak A, Muhammed GH, Mohammed AI, Hassan H. Physico-chemical Assessment of Water Quality in the Gidan Gulbi Shallow Floodplain Aquifer, Northwestern Nigeria. *American Journal of Water Resources*. 2020; 8(4): 155-163. Available from: doi:10.12691/ajwr-8-4-1.
[50] Oladipo JO, Aboyeji OS, Akinwumiju AS, Adelodun AA. Fuzzy Logic Interference for Characterization of Surface Water Potability in Ikare Rural Community, Nigeria. *Journal of Geovisualization and Spatial Analysis*. 2020; 4(1): 1-14. Available from: doi:10.1007/s41651-019-0044-z.